Chapter 2

THEORETICAL BACKGROUND

2.1 Basic Principles and Scope

The semiconductor laser diode is a forward bias *p-i-n* junction. Free carriers (electron and holes) are injected into an active region (i) by forward biasing the laser diode. In the QW strained laser diode, the active region is the strained QW layer. At low injection, these electrons and holes recombine radiatively through spontaneous emission process to emit photons. However, the laser structure is so designed that at higher injections the emission process occurs by stimulated emission. The stimulated emission process provides spectral purity to the photon output and provides coherent photons. Thus controllable change of optical properties caused by free carriers is the basic operating principle of semiconductor lasers. A typical laser structure is schematically shown in Figure 2.1.

The diode consists of a number of layers. The active region is a strained QW layer while the cladding are bulk layers. At a given ambient temperature, optical properties of the individual layer depends on its technological parameters such as material composition, width, strain, doping concentration, etc. Free carriers can be injected or doped into the layers. In active QW layer, carriers are distributed over bound states in the wells and unbound states above or below the

wells. Carrier distributions in both momentum and real spaces depend on the injection level.

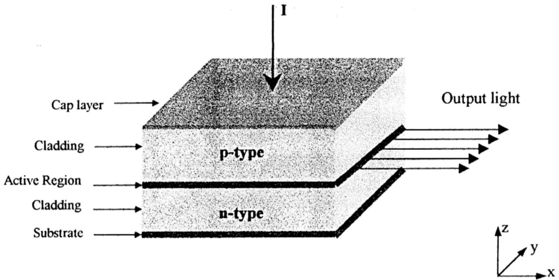

Figure 2.1 Schematic vertical structure of the injected semiconductor laser diode

In this report, the numerical methods are introduced in a natural way as needed throughout the discussion of the physics. The calculations of the optical properties are done on the basis of a semi-classical approach, which combines the macroscopic scope of the optical field, and the microscopic calculations. The optical behavior of a material is completely determined if its optical constants are known. The *complex permittivity*, κ_ω is defined by

$$\kappa_\omega = n_r^2 \tag{2.1.1}$$

where the complex refractive index, n_r consists of the real refraction index, n_ω and the extinction coefficient, k_ω is given by

$$n_r^2 = (n_\omega + ik_\omega)^2 \tag{2.1.2}$$

The n_ω affects the wavelength and velocity while k_ω gives the rate at which the wave decays with distance.

The general approach that addresses the problems of optical design and characterization in semiconductor lasers needs to be developed. The approach deals with the bulk energy structure in this chapter, then the discussion is extended to the QW and furthermore strained QW structure in next chapter. At the microscopic level, Kane model for band structure is applied, using dipole approximation for the electron-photon interaction and considering the direct (first order process) and indirect (second order process) radiative transitions. Many-body effects, such as the Coulomb and exchange-correlation interactions, are incorporated. Collective phenomena are taken into account through the effect of dynamic free carrier plasma polarization. At the macroscopic level, complex permittivity of the semiconductor layers is computed as functions of the photon energy, technological parameters, free carrier concentration and effective temperature. Then the transfer matrix method (TMM) is adopted to give the optical field distribution over the entire device. From the complex permittivity, the optical gain in semiconductor lasers can be calculated and the graphical outputs are presented.

2.2 Complex Permittivity

The complex permittivity provides all the details of the light-matter interaction in the multi-layer heterostructure device. Macroscopically, the imaginary part of the permittivity can be expressed in terms of the rate of indirect stimulated

transitions, $R_{\omega,st}$, in the case of homogeneous medium, where photons are just plane waves.

$$\kappa_{\omega}^{"} = \frac{4\pi\hbar c^2}{\omega^2} \times \frac{R_{\omega,st}}{A_{\omega}^2} \quad (2.2.1)$$

Here c is the speed of light in vacuum and A_{ω} is the real amplitude of the vector-potential of a light wave at the circular frequency ω.

Since the imaginary part of the permittivity has strong frequency dependence in the spectral range near the band gap, the radiative transitions also affect the real part of the permittivity, $\kappa_{\omega}^{'}$ in this spectral range. A modified Sellmeier equation in the form of interpolation is performed by Marple used to determine the real part of permittivity as function of the wavelength:

$$\kappa_{\lambda}^{'} = A_S + B_S\left(\frac{\lambda^2}{\lambda^2 - C_S}\right) \quad (2.2.2)$$

where λ is the wavelength measure in μm. The wavelength is related to the photon energy, E (meV) as

$$\lambda = \frac{1.2407 \times 10^3}{E} \quad (2.2.3)$$

A_S, B_S and C_S are Sellmeier coefficients defined in Appendix 1.

$\kappa_{\omega}^{'}$ is also related to $\kappa_{\omega}^{"}$ through the *Kramers-Kronig dispersion relationship*.

$$\kappa_{\omega}^{'} = \frac{2}{\pi} PV \int_0^{\infty} \frac{d\varpi\varpi}{\varpi^2 - \omega^2} \kappa_{\omega}^{"} \quad (2.2.4)$$

For practical approach, the Kramers-Kronig dispersion relationship is useful to calculate the change in $\kappa_{\omega}^{'}$ due to modification of the band structure and/or occupation numbers near the band gap. In this case, the relationship can be expressed as

PERPUSTAKAAN UNIVERSITI MALAYA

$$\Delta\kappa'_{\omega} = \frac{2}{\pi} PV \int_{0}^{\infty} \frac{d\varpi\varpi}{\varpi^{2} - \omega^{2}} \Delta\kappa''_{\omega} \tag{2.2.5}$$

where $\Delta\kappa_{\omega}$ is the change in the real part of the permittivity due to the change in imaginary part, $\Delta\kappa''_{\omega}$ in the narrow spectral range around the band gap.

In addition to the complex permittivity, two other important real parameters, the refraction index, n_{ω}, and the extinction coefficient, k_{ω} as related to complex permittivity in equation (2.1.2) are used to characterize the optical properties of the semiconductor layers. The expressions for these parameters are

$$n_{\omega} = \frac{1}{2}\left[\kappa'_{\omega} + \left(\kappa'^{2}_{\omega} + \kappa''^{2}_{\omega}\right)^{1/2}\right]^{1/2} \tag{2.2.6}$$

$$k_{\omega} = \frac{\kappa''_{\omega}}{\sqrt{2}}\left[\kappa'_{\omega} + \left(\kappa'^{2}_{\omega} + \kappa''^{2}_{\omega}\right)^{1/2}\right]^{-1/2} \tag{2.2.7}$$

k_{ω} is directly related to the absorption coefficient, α_{ω} given in cm^{-1}, which arises in the Lambert-Bouguer law

$$\alpha_{\omega} = 2(\omega/c)k_{\omega} \tag{2.2.8}$$

Instead of the absorption coefficient, the optical gain coefficient is commonly used and is defined as $$g_{\omega} = -\alpha_{\omega} \tag{2.2.9}$$

where in this case, the optical gain coefficient is the negative value of the absorption coefficient.

In order to study laser characteristics around and above threshold, the radiative current density provides an estimate of the injected current density required achieving a gain carrier density. A simple relation for the radiative current density is established as

$$J_{rad} = \frac{end}{\tau_{r}} \tag{2.2.10}$$

where e is electron charge, n is carrier density in the active region, d is the active layer thickness and τ_r is the total radiative lifetime.

2.3 Transfer Matrix Method (TMM)

After the optical properties expressed in terms of the complex permittivity of the semiconductor layers are determined, the optical characteristics of the entire multi-layer device structure can be found using *transfer matrix method* (TMM).

In classical electromagnetism, the response to an electric field is described by both a current and a polarization, which is usually absorbed into the displacement. This can be explicitly expressed in terms of the Maxwell equations. The four Maxwell equations are

$$\nabla \cdot (\hat{k}_\omega E_\omega) = 0 \tag{2.3.1}$$

$$\nabla \times E_\omega = i\frac{\omega}{c} H_\omega \tag{2.3.2}$$

$$\nabla \cdot H_\omega = 0 \tag{2.3.3}$$

$$\nabla \times H_\omega = -i\frac{\omega}{c} \hat{k}_\omega E_\omega \tag{2.3.4}$$

where E_ω and H_ω are the Fourier components of the electric and magnetic fields respectively, and $\hat{k}_\omega$ is the tensor of the complex permittivity, all at a frequency ω. Due to electronic and optical properties of QW layers are different in the directions parallel (xy-plane) and perpendicular (z-direction) to the direction of the epitaxial growth, the semiconductor layers are considered to be optically

anisotropic. Considering all the layers are homogeneous in z-direction, the complex permittivity will have the form

$$\hat{k}_\omega = \begin{bmatrix} \kappa_{\omega\perp} & 0 & 0 \\ 0 & \kappa_{\omega\perp} & 0 \\ 0 & 0 & \kappa_{\omega z} \end{bmatrix} \tag{2.3.5}$$

where $\kappa_{\omega\perp}$ and $\kappa_{\omega z}$ are the complex permittivities in the directions perpendicular and parallel to the direction of growth, respectively.

The transverse electric (TE) polarization is the electric field in the plane perpendicular to z while the transverse magnetic (TM) polarization is the magnetic field in the plane perpendicular to z. Figure 2.2 illustrates these polarization schematically.

The vectorical fields for these two modes can be expressed by a scalar function

$$\Psi_{\omega,j}(r_\perp, z) = \exp(i\beta_\perp r_\perp)\{F_{\omega,j}\exp[i\beta_{zj}(z - z_{j-1})] + B_{\omega,j}\exp[-i\beta_{z,j}(z - z_{j-1})]\} \tag{2.3.6}$$

where $\beta_\perp$ is the in-plane propagation constant, common to all the layers, $\beta_{z,j}$ is the z-direction propagation constant in j-th layer, $F_{\omega,j}$ and $B_{\omega,j}$ are the amplitudes of forward and backward propagating waves, respectively.

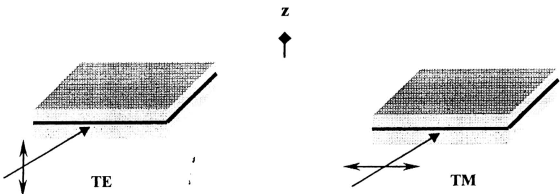

Figure 2.2 TE and TM polarization of the semiconductor laser diode

Table 2.1 tabulates all the components of the electromagnetic field in equation (2.3.6) for both the TE and TM polarization. Together with the complex permittivity in equation (2.3.5) and the scalar function in equation (2.3.7), the four Maxwell equations from (2.3.1) to (2.3.4) can be solved in every single layer in the semiconductor laser diode.

Parameter	TE polarization	TM polarization
β_z^2	$\frac{\omega^2}{c^2}\kappa_{\omega\perp} - \beta_\perp^2$	$\frac{\omega^2}{c^2}\kappa_{\omega\perp} - \frac{\kappa_{\omega\perp}}{\kappa_{\omega z}}\beta_\perp^2$
γ	1	$\frac{1}{\kappa_{\omega\perp}}$
$E_{\omega\perp}$	Ψ_ω	$-i\frac{c}{\omega}\frac{1}{\kappa_{\omega\perp}}\frac{d\Psi_\omega}{dz}$
$E_{\omega z}$	0	$-i\frac{c}{\omega}\beta_\perp\frac{1}{\kappa_{\omega z}}\Psi_\omega$
$H_{\omega\perp}$	$i\frac{c}{\omega}\frac{d\Psi_\omega}{dz}$	Ψ_ω
H_ω	$\frac{c}{\omega}\beta_\perp\Psi_\omega$	0

Table 2.1 Propagation constant in z-direction and electromagnetic field

At the interfaces, standard boundary conditions for electric and magnetic fields yield the following transfer relationship for the scalar function (2.3.6) and its derivative

$$\Psi_{\omega,j} = \Psi_{\omega,j-1} \tag{2.3.7}$$

$$\gamma_j \frac{d\Psi_{\omega,j}}{dz} = \gamma_{j-1} \frac{d\Psi_{\omega,j-1}}{dz} \tag{2.3.8}$$

where the factor γ is defined in Table 2.1.

Combining equations (2.3.6), (2.3.7) and (2.3.8), the amplitudes of the forward and backward propagating waves can be determined by

$$\begin{bmatrix} F_{\omega,j} \\ B_{\omega,j} \end{bmatrix} = \hat{T}_{\omega j} \begin{bmatrix} F_{\omega,j-1} \\ B_{\omega,j-1} \end{bmatrix} \tag{2.3.9}$$

where $\hat{T}_{\omega j}$ is a square 2 x 2 complex transfer matrix, defined by

$$\hat{T}_{\omega j} = \begin{bmatrix} \frac{1}{2}(1+\zeta_j)\exp(i\Delta_j) & \frac{1}{2}(1-\zeta_j)\exp(-i\Delta_j) \\ \frac{1}{2}(1-\zeta_j)\exp(i\Delta_j) & \frac{1}{2}(1+\zeta_j)\exp(-i\Delta_j) \end{bmatrix} \tag{2.3.10}$$

where the complex parameters ζ_j and Δ_j are defined as follows:

$$\zeta_j = \frac{\beta_{z,j-1}\gamma_{j-1}}{\beta_{z,j}\gamma_j} \tag{2.3.11}$$

$$\Delta_j = \beta_{z,j} d_j \tag{2.3.12}$$

The amplitudes of the plane waves in cap layer and substrate can be obtained through the multiplication of the matrixes in equation (2.3.10):

$$\begin{bmatrix} F_{\omega,n+1} \\ B_{\omega,n+1} \end{bmatrix} = \hat{T}_{\omega} \begin{bmatrix} F_{\omega,0} \\ B_{\omega,0} \end{bmatrix} \tag{2.3.13}$$

where
$$\hat{T}_{\omega} = \prod_{j=1}^{n} \hat{T}_{\omega j} \tag{2.3.14}$$

The TMM can solve the optical field distribution over the entire laser diode after the boundary conditions in the substrate $(z \to -\infty)$ and cap layer $(z \to \infty)$ are specified. This completes the macroscopic part of the calculations. The following parts will deal with the microscopic level of the approach.

2.4 The Rate of Stimulated Transitions

The key understanding the semiconductor laser diode is the physics behind the stimulated emission. This radiative process is related to the number of participating quasi-particles other than electrons. In the first order process, the electron transition results from an interaction with only one photon, which is also termed direct one photon transition. In the second order process, impurity or phonon scattering is involved, and it is termed indirect impurity or phonon-assistant transition.

The rate of direct stimulated transitions at the photon energy $\hbar\omega$ is obtained by using the *Fermi's golden rule* which governs the first order perturbation theory :

$$R^{(1)}_{\omega,st} = \frac{\pi e^2 A^2_\omega}{\hbar m^2_o c^2} \sum_{(i,f)} |P_{fi}|^2 (f_i - f_f)\delta_\Gamma(E_f - E_i - \hbar\omega) \quad (2.4.1)$$

Here, e and m_o are the charge and mass of a free electron, respectively, P_{fi} is the matrix element for electron's momentum in the direction of the vector potential, E_i , f_i and E_f, f_f are the energies and occupation numbers of the initial and final states, respectively.

δ_Γ is the broadened energy delta function which is taken as

$$\delta_\Gamma(E_f - E_i - \hbar\omega) = \frac{1}{\pi\Gamma} \frac{1}{\cosh[(E_f - E_i - \hbar\omega)/\Gamma]} \quad (2.4.2)$$

with Γ denotes as a parameter of broadening which is related to the coherence time τ involved in a transition by

$$\Gamma = \frac{2\pi\hbar}{\tau} \quad (2.4.3)$$

In this case, the delta function is approached as the coherence time τ increases to infinity, then $\Gamma \to 0$.

The rate of indirect stimulated transitions are obtained from the second order perturbation theory as:

$$R_{\omega a}^{\pm} = \frac{\pi e^2 A_\omega^2}{\hbar^3 m_o^2 c^2 \omega^2} \sum_{(i,f)} f_i (1-f_f) |V_{fi}|^2 \left| \langle f | \hat{H}_\Omega^{\pm} | i \rangle \right|^2 \delta_\Gamma (E_f - E_i - \hbar\omega \mp \hbar\Omega) \qquad (2.4.4)$$

$$R_{\omega e}^{\pm} = \frac{\pi e^2 A_\omega^2}{\hbar^3 m_o^2 c^2 \omega^2} \sum_{(i,f)} f_i (1-f_f) |V_{fi}|^2 \left| \langle f | \hat{H}_\Omega^{\pm} | i \rangle \right|^2 \delta_\Gamma (E_f - E_i + \hbar\omega \mp \hbar\Omega) \qquad (2.4.5)$$

Here, $|i\rangle$ and $\langle f|$ denote the initial and final states of electrons, respectively. The subscripts "a" and "e" indicates the photon absorption and emission processes respectively, while the processes of absorption and emission of the phonon are indicated by superscripts "+" and "-" respectively.

$$V_{fi} \equiv v_f - v_i \qquad (2.4.6)$$

where v_f and v_i are the quantum-mechanical velocities of the electron in those states, which are defined as

$$v_j \equiv \frac{1}{m_o} \langle j | \hat{p} | j \rangle, \quad j = i, f \qquad (2.4.7)$$

$\hat{H}_\Omega^{\pm}$ in equations (2.4.2) and (2.4.3) is the Hamiltonian of the electron interaction with the phonon and/or ionized impurity, with the energy $\hbar\Omega$. And the rate of indirect stimulated transitions at photon energy $\hbar\omega$ is the sum of equations (2.4.2) and (2.4.3).

$$R_\omega^{(2)} = R_{\omega a}^{\pm} + R_{\omega e}^{\pm} \qquad (2.4.8)$$

Thus, the resultant rate of stimulated transitions is the combined rate of the first and second order processes:

$$R_{\omega,st} = R_{\omega,st}^{(1)} + R_{\omega,st}^{(2)} \qquad (2.4.9)$$

Substitution of the rate of stimulated transitions obtained in equation (2.4.9) to equation (2.2.1) yields the imaginary part of the permittivity as:

$$\kappa_{\omega}^{''} = \frac{4\pi^2 e^2}{m_o^2 \omega^2} \sum_{(i,f)} \Big[|P_{fi}|^2 (f_i - f_f)\delta_\Gamma(E_f - E_i - \hbar\omega) + |V_{fi}|^2 f_i(1-f_f) \sum \left| \langle f | \hat{H}^{\pm}_{\Omega_s} | i \rangle \right|^2 \delta_\Gamma(E_f - E_i \mp \hbar\omega \mp \hbar\Omega_s) \Big] \tag{2.4.10}$$

Until now, the complex permittivity obtained are general without taking into account the effects of many-body effect such as the excitonic absorption and band gap shrinkage or the collective effects such as dynamic polarization of free carrier plasma and the carrier-induced anomalous dispersion. All these effects will be incorporated in the model phenomenologically in the following sections.

2.5 The Kane Model

This celebrated *Kane model*[12] is an extension of $\boldsymbol{k}\,.\,\boldsymbol{p}$ method. In this method, the perturbation Hamiltonian is proportional to the scalar product of the operator of momentum and the wave-vector of the Bloch electron, hence it is known as the $\boldsymbol{k}\,.\,\boldsymbol{p}$ method. This method aims to obtain a more accurate description of the bands near the top of the valence band and the bottom of the conduction band rather than the parabolic approximation for these bands.

Bloch's theorem states that the wave function in a crystal can be written as the product

$$\Psi_i(r) = \frac{\exp(ikr)}{\sqrt{V}} u_{ik}(r) \tag{2.5.1}$$

where r is the coordinate vector, V is the volume of the crystal, and $u_{ik}(r)$ is the periodic function of r with the same period as that of the crystal lattice. This function is never known exactly, thus approximate methods have to be applied. The approach of Kane model will be adopted under this circumstance. This model takes into account four double degenerated bands, i.e. conduction band (c-) along with heavy (vh-), light (vl-) and split off (vs-) valence bands. All of them is considered to be isotropic and follows the dispersion law as follows:

$$\frac{\hbar^2 k^2}{2m_i} = \gamma_i(\varepsilon) = \varepsilon(1 + a_i\varepsilon) \tag{2.5.2}$$

where m_i and a_i are the band-edge effective mass and parameter of nonparabolicity in i-th band, respectively, and ε is the energy relative to the band edge. All the valance bands are considered to be parabolic, thus a_i is set to be zero for i = vh, vl and vs. For the conduction band, the parameter of nonparabolicity is derived from the Kane model:

$$a_\Gamma = \frac{(1+\chi/3)(1+\chi) + \chi^2/3}{(1+2\chi/3)(1+\chi)} \frac{1}{E_g} \tag{2.5.3}$$

where

$$\chi = \frac{E_{so}}{E_g} \tag{2.5.4}$$

Here, E_g denotes the energy gap between the conduction and valence bands and E_{so} is the spin-splitting energy in the valence band. The subscript "Γ" indicates the central Γ-valley of the conduction band. Besides this, as illustrated in Figure 2.3, there are another two minimums in the conduction band of III-V semiconductor, denoted the side X- and L-valleys. The overall density of states are much larger than that in the Γ-valley and follows the same dispersion law as the Γ-valley. They also play an important role in the position of the quasi-Fermi

level and intraband scattering in the conduction band. As a result, there are six different sorts of charge carriers existing, i.e. Γ, X and L electrons along with heavy (vh), light (vl) and split-off (vs) holes. Also, there are overall six different types of charge carrier transitions among the bands. These are the direct interband transitions as indicated by arrows in Figure 2.3. Three of these transitions occur between the valence bands and the conduction band, while another three transitions are the intervalence band transitions.

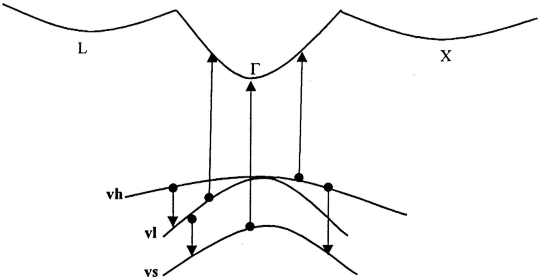

Figure 2.3 Schematic band structure of direct gap III-V semiconductor

PERPUSTAKAAN UNIVERSITI MALAYA

2.5.1 Distribution Functions

The quasi-equilibrium Fermi-Dirac distribution function used to describe all the electrons and holes over the Bloch states in the conduction and valence bands, respectively, is expressed as follows :

$$f_{ij}(\varepsilon) = \left[1 + \exp\left(\frac{\Delta_{ij} + \varepsilon}{T_i} - \xi_i\right)\right]^{-1} \tag{2.5.5}$$

where j denotes the sort of carriers and i denotes the band involved. Δ_{ij} is the separation energy between the i-th band and the reference point. T_i is the effective temperature of carriers in the i-th band. ξ_i is the normalized chemical potential of the conduction or valence band and is defined by

$$\xi_i = \begin{cases} (\Phi_c - E_c)/T_c & i = c \\ -(\Phi_v - E_v)/T_v & i = v \end{cases} \tag{2.5.6}$$

Here, Φ_c and Φ_v are the Fermi levels of conduction and valance bands, respectively, E_c and E_v denote the band-edge energies.

The normalized chemical potential can be resolved from the carrier concentration, N_i as follows:

$$N_i = \sum_{(j)} \aleph_{ij,3D}(T_i) \frac{2}{\sqrt{\pi}} \int_0^\infty \frac{du u^{\frac{1}{2}} \rho_{ij}(u)}{1 + \exp\left(\xi_i - \frac{\Delta_{ij}}{T_i} - u\right)} \tag{2.5.7}$$

where the density of states is defined as

$$\aleph_{ij}(T_i) = 2\nu_{ij}\left[\frac{2\pi m_{ij} T_i}{(2\pi\hbar)^2}\right]^{\frac{3}{2}} \tag{2.5.8}$$

$$u = \frac{\varepsilon}{T_i} \tag{2.5.9}$$

and the reduced density of states in the band is defined by

$$\rho_{ij}(\varepsilon) = \left[\gamma_{ij}(\varepsilon)\right]^{\frac{1}{2}} \frac{d\gamma_{ij}(\varepsilon)}{d\varepsilon} \qquad (2.5.10)$$

2.5.2 Direct Interband Transitions

As illustrated in Figure 2.3, there are six kinds of direct interband transitions. Only the direct radiative transitions between the valence bands and the conduction band are allowed to occur at $k = 0$. However, the intervalence band transitions occur at $k \neq 0$.

The momentum matrix element for the direct transitions can be determined by the cell periodic functions as follows:

$$P_{ij}(k) = \left\langle u_{jk} \middle| e\hat{p} \middle| u_{ik} \right\rangle \qquad (2.5.11)$$

The Kane parameter E_p is introduced through the following expression

$$\frac{1}{4\pi}\int_0^{\pi} d\vartheta \sin\vartheta \int_0^{2\pi} d\varphi \left|P_{ij}(k)\right|^2 = \frac{m_o E_p}{6} \Pi_{ij}(k) \qquad (2.5.12)$$

where the square 4 x 4 matrix of dimensionless coefficients is expressed by

$$\hat{\Pi} = \begin{bmatrix} 0 & 1 & 1 & 1 \\ 1 & 0 & 2Q^2 & (1+\chi)^{-2}Q^2 \\ 1 & 2Q^2 & 0 & (1+\chi)^{-2}Q^2 \\ 1 & (1+\chi)^{-2}Q^2 & (1+\chi)^{-2}Q^2 & 0 \end{bmatrix} \qquad (2.5.13)$$

in which the rows and columns correspond to c-, vh-, vl-, and vs-bands, respectively.

$$Q^2 \equiv \frac{1}{3}\frac{E_p}{E_g}\frac{\hbar^2 k^2}{2m_o E_g} \qquad (2.5.14)$$

Now, replace the sum over the states with integral over $d\varepsilon_k = d(\hbar^2 k^2 / 2\mu_{ij})$ in the equation (2.4.8), with μ_{ij} is the band-edge reduced effective mass. Hence from the contribution of interband transitions, the imaginary part of permittivity yields

$$\kappa''_{\omega,ib} = \frac{2^{3/2} e^2 E_p}{3 m_o \hbar^3 \omega^2} \sum_{(j=vh,vl,vs)} \mu_{cvj}^{3/2} \int_0^\infty d\varepsilon_k \varepsilon_k^{1/2} \left[1 - f_{vj}\left(\varepsilon_{vj}(\varepsilon_k)\right) - f_c\left(\varepsilon_c(\varepsilon_k)\right)\right] \delta_\Gamma \left[\varepsilon_{vj}(\varepsilon_k) + \varepsilon_c(\varepsilon_k) + E_g - \hbar\omega\right] \quad (2.5.15)$$

with

$$\varepsilon_{vj}(\varepsilon_k) = \Delta_{vj} + \frac{\mu_{cvj}}{m_{vj}} \varepsilon_k \qquad \varepsilon_c(\varepsilon_k) = \sqrt{\frac{1}{4a_\Gamma^2} + \frac{\mu_{cvj}}{m_{c\Gamma}} \frac{\varepsilon_k}{a_\Gamma}} - \frac{1}{2a_\Gamma} \quad (2.5.16)$$

On the other hand, the contribution of the intervalence band transitions to the imaginary part of permittivity is expressed as follows:

$$\kappa''_{\omega,ivb} = \frac{2^{3/2} e^2 E_p}{3 m_o \hbar^3 \omega^2} \sum_{(j=vh,vl,vs)} \mu_{cvj}^{3/2} \int_0^\infty d\varepsilon_k \varepsilon_k^{1/2} \Pi_{ij}(\varepsilon_k) \left[f_{vi}(\varepsilon_k) - f_{vj}(\varepsilon_k)\right] \delta_{\mathrm{I}} \left[\varepsilon_{vj}(\varepsilon_k) - \varepsilon_{vi}(\varepsilon_k) - \hbar\varpi\right] \quad (2.5.17)$$

with

$$\varepsilon_{vi}(\varepsilon_k) = \Delta_{vi} + \frac{\mu_{vij}}{m_{vi}} \varepsilon_k \qquad \varepsilon_{vj}(\varepsilon_k) = \Delta_{vj} + \frac{\mu_{cvj}}{m_{vj}} \varepsilon_k \quad (2.5.18)$$

The energy gap Δ_{vi} is nonzero only for the transitions involving the split-off valence band, in which $\Delta_{vs} = E_{so}$.

2.5.3 Indirect Intraband Transitions

In the previous section (2.4), the indirect radiative transitions involving impurity or phonon within the conduction or valence bands, the free carrier at the states in which energy is higher than $\hbar\omega \pm \hbar\Omega$ are neglected since their occupation numbers are small. In this section, the contribution of these free carrier processes with the absorption of photon to the imaginary part of permittivity is included. In the high energy limit, the imaginary part of permittivity is independent on energy. Thus the free carrier contribution to the imaginary part of permittivity can be simplified to

$$\kappa^{''}_{\omega,fc} \cong \frac{\omega}{c} \sum_{(i)} N_i \sum_{(s)} \mathrm{E}_{is} \qquad (2.5.19)$$

where E_{is} is the characteristic cross-section of absorption by the i-th sort carrier accompanied with scattering by the s-th type phonon. In this case, the energy $\hbar\Omega_s$ in equation (2.4.10) is set to zero since it has already been incorporated in E_{is}. Table 2.2 tabulates the characteristic cross-sections corresponding to different types of deformation phonons scattering. The related parameters described in Table 2.2 are defined in Appendix 1 and 2.

Mechanism	*Characteristic Cross-section* E_{is}	*Parameter Description*
Ionized impurities	$\frac{16\sqrt{2}\pi^2 e^6 N_{\Pi}}{3c\kappa_o^2 m_i^3 \hbar^{3/2}\omega^{7/2}}$	N_{Π} = concentration of ionized impurities
Deformation Acoustic Phonons	$\frac{4\sqrt{2}e^2 D_A^2 T_o m_i^{1/2}}{3c\rho s^2 \hbar^{7/2}\omega^{7/2}}$	D_A = acoustic deformation potential, ρ = crystal density, s = velocity of sound
Polar Acoustic Phonons	$\frac{e^4 K_{pz}^2 T_o}{3\sqrt{2}\pi c\kappa_o m_i^{1/2}\hbar^{5/2}\omega^{5/2}}$	K_{pz} = electromechanical coupling constant
Deformation Optical Phonons	$\frac{2\sqrt{2}e^2 D_o^2 m_i^{1/2}}{3c\rho\Omega_o \hbar^{5/2}\omega^{3/2}}\coth\left(\frac{\hbar\Omega_o}{2T_o}\right)$	D_o = optical deformation potential, $\hbar\Omega_o$= optical phonon energy
Polar Optical Phonons	$\frac{4\pi\sqrt{2}e^4(\kappa_\infty^{-1}-\kappa_0^{-1})\Omega_o}{3cm_i^{1/2}\hbar^{3/2}\omega^{5/2}}\coth\left(\frac{\hbar\Omega_o}{2T_o}\right)$	κ_o, κ_∞ = low- and high-frequency limits of the permittivity, respectively
Inter-valley Optical Phonons	$\frac{2\sqrt{2}e^2 D_{ij}^2 m_j^{1/2}(\hbar\omega-\Delta_{ij})^{3/2}}{3c\rho\hbar^4\Omega_{ij}\omega^3}\coth\left(\frac{\hbar\Omega_{ij}}{2T_o}\right)$	D_{ij} = inter-valley optical deformation potential, $\hbar\Omega_{ij}$ = inter-valley optical phonon energy

Table 2.2 Characteristic cross-sections of the phonon assistant indirect intraband transitions

2.5.4 Many-Body and Collective Effects

Many-body and collective effects are not incorporated in the derivation of the imaginary part of permittivity expressed previously. Two important kinds of the many-body effects are the Coulomb interaction and exchange-correlation interaction while the collective effects come from the dynamic plasma polarization and anomalous dispersion.

The Coulomb interaction between the electron and hole modifies their states thus excitonic transitions are possible below the band gap at low concentrations of free carriers. The excitonic transitions are incorporated by the term[4] [15]:

$$\kappa''_{\omega,ex} = \frac{2\pi^2 e^2 E_p}{m_o \omega^2} \tanh\left[\frac{1}{2}\left(\frac{\hbar\omega - E_g}{T_c} + \frac{\hbar\omega - E_g}{T_v} - \xi_c - \xi_v\right)\right] \sum_{(h,l)} \sum_{(n)} \left|\Psi_{jn}\right|^2 \delta_\Gamma(\varepsilon_{jn} + E_g - \hbar\omega) \tag{2.5.20}$$

On the other hand, the exchange-correlation interaction is apparent at high carrier concentrations. This results in the lowering the bottom of the conduction band and raising the top of the valence band, which causes band gap shrinkage. The shift of band edge can be described by

$$V_{xc,j}(N_j) = 0.0582\left(1 + 0.7734\eta_j^{-1}(N_j)\ln\left[1 + \eta_j(N_j)\right]\right)\eta_j(N_j)R_j \qquad \text{j = c, vh, vl} \tag{2.5.21}$$

Here, the number of j-th band carriers in a spherical volume a radius equal to the effective Bohr radius $a_{B,j}$ is defined as

$$\eta_j = 21\left(\tfrac{4}{3}\pi a_{B,j}^3 N_j\right)^{1/3} \tag{2.5.22}$$

$$a_{B,j} = \frac{\kappa_o \hbar^2}{m_j e^2} \tag{2.5.23}$$

and R_j is the effective Rydberg constant in that band, defined by

$$R_j = \frac{e^2}{2\kappa_o a_{B,j}} \tag{2.5.24}$$

Then, the band gap shrinkage is the sum of the conduction and valence band shifts,

$$\Delta E_{g,xc} = V_{xc,c}(N_c) + V_{xc,v}(N_v) \tag{2.5.25}$$

In the electric field of optical radiation, the dynamic polarization of free carrier plasma also contributes change in the real part of permittivity. This change can be approximated as follows :

$$\Delta\kappa'_{\omega,pl} \cong -\frac{4\pi e^2}{\omega^2}\sum_{(i)}\frac{N_i}{m_i} \tag{2.5.26}$$

Due to the strong spectral dependence of absorption near the band edge, anomalous dispersion is another effect induced that changes the real part of permittivity. By applying the integral Kramers-Kronig dispersion relationship, the change forms

$$\Delta\kappa'_{\omega,ad}(N,T) = \frac{2}{\pi}PV\int_0^\infty \frac{d\varpi\varpi}{\varpi^2-\omega^2}\left[\kappa''_\varpi(N,T) - \kappa''_\varpi(N_o,T_o)\right] \tag{2.5.27}$$

where N, T are the carrier concentrations and temperatures, respectively while N_o, T_o are related to equilibrium carriers due to residual doping.

After going through the derivation the complex permittivity using the approach of Kane Model and incorporated with the many-body effects, the total imaginary part of permittivity can be calculated with

$$\kappa''_\omega = \kappa''_{\omega,tb} + \kappa''_{\omega,ex} + \kappa''_{\omega,ivb} + \kappa''_{\omega,fc} \tag{2.5.28}$$

2.6 Summary

In this chapter, basic concepts from physics and the theoretical backgrounds linked directly to the simulation of the model are complied to provide computations and derivations of the optical properties of the modeled structure. In this part, the approach deals with the bulk energy structure. This theory will be elaborated to the quantum well and furthermore strained quantum well structure in next chapter. Microscopically, Kane model for band structure are applied, using dipole approximation for the electron-photon interaction and considering the direct (first order process) and indirect (second order process) radiative transitions. Many-body effects, such as the Coulomb and exchange-correlation interactions, are incorporated. Collective phenomena are taken into account through the effect of dynamic free carrier plasma polarization. Macroscopically, complex permittivity of the semiconductor layers is derived and the optical properties such as optical gain and propagation constant can be calculated. Then the transfer matrix method (TMM) is adopted to give the optical field distribution over the entire device.